ADAR1 Prevents R-loop Accumulation-Driven ATR Pathway Activation in Ovarian Cancer

hanwei cui
Shenzhen Second People's Hospital
Qian Yi
Shenzhen Second People's Hospital
Min Tian
Third Military Medical University Daping Hospital and Research Institute of Surgery
Yuteng Liang
Shenzhen Second People's Hospital
Jie Huang
Third Military Medical University Daping Hospital and Research Institute of Surgery
Qi Zeng
Third Military Medical University Daping Hospital and Research Institute of Surgery
Weichao Sun
Third Military Medical University Daping Hospital and Research Institute of Surgery
Jian Han
Third Military Medical University Daping Hospital and Research Institute of Surgery
Jianxin Guo
Third Military Medical University Daping Hospital and Research Institute of Surgery
Zhiying Yu
Shenzhen Second People's Hospital
Wenlan Liu (wlliu@szu.edu.cn)
Shenzhen Second People's Hospital
Xiufeng Ye
Shenzhen Second People's Hospital

Research

Keywords: Ovarian Cancer, ADAR1, DNA Damage, R-Loop

Posted Date: November 12th, 2020

DOI: https://doi.org/10.21203/rs.3.rs-103651/v1

Abstract

Background

Adenosine (A)-to-inosine (I) RNA editing is the most prevalent RNA editing mechanism, in which adenosine deaminases acting on RNA 1 (ADAR1) is a major adenosine deaminase. Increasing evidence suggests that editing dysregulation of ADAR1 plays an important role in human tumorigenesis, while the underlying mechanism remains elusive.

Methods

The clinical relevance of ADAR1 was analyzed by real-time PCR, western blotting and immunohistochemistry of ovarian cancer tissues. ADAR1 function on ovarian cancer cells in vitro were explored by colony formation assay, transwell assay and Brdu-based cell cycle assay in vitro and xenograft models in vivo. Western blotting, immunostaining and DNA/RNA immunoprecipitation-qPCR were conducted to confirm DNA damage and R-loop accumulation in ovarian cancer cells. Co-immunoprecipitation and DNA/RNA immunoprecipitation were performed to detect interaction of DHX9, ADAR1 and R-loop complex in ovarian cancer cells.

Results

We demonstrated that ADAR1 was highly expressed in ovarian cancer tissues and negatively correlated with progression free survival of ovarian cancer patients. Importantly, silence of ADAR1 repressed ovarian cancer cell growth and colony formation in vitro and inhibited ovarian cancer cell tumorigenesis in vivo. Further cell cycle and transcriptome profile analysis revealed that silence of ADAR1 in ovarian cancer cells induced cell cycle arrest at G1/G0 stage. Mechanically, loss of ADAR1 caused R-loop abnormal accumulation, thereby contributing to single stand DNA break and ATR pathway activation. Additionally, ADAR1 interacted with DHX9 to regulate R-loop complex formation, and A-to-I editing of nascent RNA repressed R-loop formation during co-transcriptional process.

Conclusions

Our results identify a novel ADAR1/R-loop/ATR axis critical for ovarian cancer progression and a potential target for ovarian cancer therapy.

Background

Ovarian cancer is the most lethal malignant tumor in gynecological cancers with a poor 5-year survival rate of only 28% in advanced stages[36]. The standard treatment for ovarian cancer is cytoreductive surgery and taxane/platinum based chemotherapy. However, more than 70% of patients with advanced stages recur within 5 years and develop drug resistance after standard treatment[5]. Thus, it's critical to identifying more effective treatment strategies and novel molecular targeting agents for improving survival rates for patients with ovarian cancer.

Adenosine (A) to inosine (I) RNA editing is the most prevalent RNA editing mechanism in human, which is catalysed by double-stranded RNA (dsRNA)-specific adenosine deaminase (ADAR) protein family (ADAR1, ADAR2 and ADAR3)[39]. Recent studies indicated that ADAR1 was upregulated in several cancers, including hepatocellular carcinoma [9], esophageal cancer[30, 42], leukemia[31], and lung cancer[2, 34], due to amplification of ADAR1 gene locus or activation of JAK-STAT pathway. Further studies have revealed that hyper editing of different types of RNA by ADAR1, including mRNA and non-coding RNA, contributes to the malignant phenotype, or even cancer progression[15, 40]. Besides RNA editing function, other functions of ADAR1 have also been explored, including forming a complex with DICER to regulate microRNA processing[28], competing with STAUFEN to prevent mRNA-decay[32]. Recently, loss of ADAR1 was reported to cause hyperactivation of PKR and translational shutdown[12], and even overcome resistance to immune checkpoint blockade treatment in a subset of cancer cell lines [17, 20].

In spite of the growing evidence for A-to-I RNA editing in tumorigenesis, the clinical significance and the functional role of ADAR1 in ovarian cancer remains unexplored. Herein, we found that ADAR1 was significantly upregulated in ovarian cancer tissue and knockdown of ADAR1 repressed ovarian cancer cell line tumorigenesis through inducing cell cycle arrest. Further mechanistic experiments revealed that repression of ADAR1 did not activate PKR and type 1 IFN pathway, but rather caused single strand DNA break and abnormal R-Loop accumulation. Our data shed new light on the role of ADAR1 in promoting carcinogenesis in ovarian cancer.

Materials And Methods

Patients and specimens

Serous epithelial ovarian cancer tissues were obtained from patients who were subjected to surgical resection in the department of Gynecology & Obstetrics, Daping Hospital, Army Medical University (Chongqing, China) between 2015 and 2018. No antitumor treatment was given before the surgery. Fresh ovarian surface epithelium brushings were obtained from the normal ovaries of donors during surgery for other benign gynecological diseases at Daping hospital between 2015 and 2018. All samples were frozen into liquid nitrogen within 10 min after surgical resection and stored at -80℃ until analyses. Tissue array blocks containing ovarian cancer and normal ovarian tissues were established using a tissue microarrayer (Leica, Germany). Procedures for the collection of human samples and their usage for tissue arrays were approved by the Ethical Committee of the Army Medical University (Chongqing, China). All patients signed an informed consent for participating in this study.

Cell Culture

HEK293T, A2780, IGROV1 and SKOV3 were purchased from Procell Life Science & Technology Co., Ltd (Wuhan, China). All cells were identified by short tandem repeat (STR) profiling and cultured according to the manufacturer's specifications for less than 3 months. HEK293T, A2780 and IGROV1 cells were cultured in Dulbecco's modified Eagle's medium (Gibco, China) containing 10% fetal bovine serum (Gibco,

USA) and 1% penicillin (Gibco, USA). SKOV3 cells were cultured in McCoy's 5A medium (Gibco, China) containing 10% fetal bovine serum and 1% penicillin. All cell lines were tested mycoplasma negative and cultured in an incubator (Thermo Fisher, USA) gassed with 5% CO2 at 37 °C.

Plasmid Construction and Lentiviral Packing

pLKO.1 vector (Addgene, USA) was used for ADAR1 short hairpin RNA targeted ADAR1 and the negative control with non-target. pcDNA3.1(+) (Invitrogen, USA) vector was used for ADAR1 overexpression. ADAR1 with E912A mutation was generated using Mut Express MultiS Fast Mutagenesis Kit (Vazyme, China). The lentivirus was generated following the manufacturer's instructions. Briefly, pLKO.1 vector, psPAX2 and pMD2.G plasmids (Addgene, USA) were co-transfected into HEK293T cells using lipofectermineTM 2000 (Invitrogen, USA). Viral supernatants were collected and filtrated using 0.45 um filter. The lentivirus was used immediately or stored at −80 °C. Target cells were infected by lentivirus with 8 ug/ml polybrene (Sigma, USA) and then selected by 2 ug/ml puromycin (Coring, USA) for 5 days to gain the stable cell line. The related sequences of shRNAs and PCR primer were shown in Supplementary Table 1.

Cell Proliferation and Colony Formation

For cell proliferation assay, SKOV3, A2780 and IGROV1 cells were seeded at 10000 cells/well into 6-well plates. Cell numbers were counted by TC10 Automated Cell Counter in every two days. Growth curves were plotted using data from three independent biological replicates. For colony formation assay, SKOV3, A2780 and IGROV1 cells were seeded at 500 cells/well into 6-well plates, and then cultured for 14 days in medium containing 10% FBS at 37 °C. The colonies were fixed with methanol and stained with 0.5% crystal violet. The number of colonies were counted under an inverted microscope.

Cell Migration Assay

A total of 40,000 SKOV3 cells or 80,000 A2780 cells were used for experiment respectively. Cell suspensions (300 ml) without FBS were plated in the upper non-matrigel-coated chamber, and fresh medium containing 10% FBS was added into the lower chamber. After 24 hours of incubation, the cells across the 8 mm size hole were fixed by incubation with methyl alcohol for 15 min and then stained with crystal violet. Microscopic images were randomly taken under a microscopy and the mean number of migrated cells in each well was calculated from at least three random fields.

Cell Cycle Assay

BrdU based cell cycle analysis was performed using BrdU Flow Kit (ebiosciences, BD, USA) according to the manufacturer's instructions. Briefly, SKOV3 and A2780 cells were cultured for 30 min with 10 mM BrdU. The cells were fixed, permeabilized and then treated with DNase to expose incorporated BrdU. After incubation with anti-BrdU antibodies and 7-AAD, and the cells were subjected to flow cytometer analysis (CytoFLEX, Beckman,USA). Cell-cycle distribution was analyzed using FlowJo software (FlowJo).

RNA Isolation and Quantitative real-time PCR

For gene expression analysis, total RNA was isolated from cells using RNeasy Mini Kit (Qiagen, German) and reverse-transcribed to complementary DNA using PrimeScript™ RT-PCR Kit (Takara, China). Quantitative real-time PCR (qRT-PCR) was performed using SYBR® Green Master Mix (Bio-Rad, USA). Individual values were normalized to house-keeping gene GAPDH that served as an internal control. Relative mRNA expression levels were calculated using the $2^{-\Delta\Delta CT}$ method. Primers used in RT-qPCR were listed in Supplementary Table S1.

RNA Sequencing (RNA-seq)

A total amount of 2 μg RNA per sample was used as input material for the RNA sample preparations. Sequencing libraries were generated using VAHTSTM mRNA-seq V2 Library Prep Kit for Illumina® (Vazyme, China) following manufacturer's recommendations and index codes were added to attribute sequences to each sample. Paired-end sequencing of the library was performed on the HiSeq XTen sequencers (Illumina, San Diego, CA). Sequence reads were mapped to the human genome version hg38 by using Illumina sequence analysis pipeline.

Western Blot Analysis

Cellular proteins were extracted using SDS lysis buffer, separated by 10% SDS–polyacrylamide gel electrophoresis, transferred onto polyvinylidene difluoride membranes and then blocked with 5% defatted milk. After incubation with indicated primary antibodies (1:1000 dilution) at 4 °C overnight and anti-goat or anti-rabbit secondary antibodies (Cell Signaling Technologies, USA) at room temperate for 2 hours, immunoreactive signal was visualized using ECL detection kit (Millipore, USA) according to the manufacturer's instructions.

Immunofluorescence Staining

The cells were fixed in 4% paraformaldehyde (PFA) for 20 min, blocked with 0.1% Triton X-100 for 1 hours at 25 °C, and then incubated with γ-H2AX antibody (Cell Signaling Technologies, USA) or S9.6 antibody (Kerafast, USA) overnight at 4 °C, followed by Alexa FluorR 488 or 594 goat anti-rabbit IgG secondary antibody (H + L) (Proteintech, China) for 2 hours at room temperate. The nuclei were stained with 300 nM DAPI (Proteintech, China) for 15 min at 25 °C.

Immunohistochemistry (IHC) Assay

For IHC assays, paraffin-embedded tissue sections were probed with ADAR1 and Ki67 antibodies (1:100) at 4 °C overnight, and then incubated with SignalStain Boost IHC Detection Reagent (horseradish peroxidase, mouse) (Cell Signaling Technologies, USA) at room temperature for 15 min. DAB Horseradish Peroxidase Color Development Kit was used for staining visualization, and hematoxylin was used for tissue counterstain. IHC staining was evaluated using a semiquantitative scoring method. Each sample was graded on the basis of the H-score (H-score = I × P, where I was the staining intensity score and P was

the score for the percentage of positively stained cells at each staining intensity level). The I scores were defined as follows: 0, no staining; 1, weak staining; 2, moderate staining; and 3, strong staining. The P scores were defined as follows: 0, <5%; 1, 5–25%; 2, 26–50%; 3, 51–75%; and 4, >75%.

Immunoprecipitation

Each sample used 5×10^6 cells, which were lysed in cell lysis buffer (50mM Tris-Cl, 2mM EDTA, 137 mM NaCl, 1% Nonidet P-40). The cell lysates were incubated with indicated antibodies (5 mg) overnight at 4°C and then incubated with 25 ml protein A/G beads (Thermo Fisher, USA) for 4 h at 4°C. The beads were washed three times with lysis buffer and immunocomplexes were eluted by 1×SDS loading buffer for 20 min. The collected proteins were transferred to PVDF membrane and immunoblotted with indicated antibodies.

DNA/RNA Immunoprecipitation (DRIP) and DRIP-qPCR

For DRIP, 10^7 cells per sample were lysed in cell lysis buffer (50mM Tris-Cl, 2mM EDTA, 137 mM NaCl, 0.5% Trixon X-100). The cell lysates were incubated with S9.6 antibody overnight at 4°C and then with 50 ml protein A/G beads (Thermo Fisher) for 4 h at 4 °C. During incubation, 0.5 ng RNase A (PureLink, Invitrogen) was added to digest RNA when needed. The beads were washed three times with lysis buffer and immunocomplexes were eluted by 1×SDS loading buffer for 20 min. The collected proteins were transferred to PVDF membrane and immunoblotted using proper antibodies.

For DRIP-qPCR, 10^7 cells per sample were lysed in cell lysis buffer (10 mM Tris-Cl, 1mM EDTA, 0.5% SDS). Nucleic acid was extracted by phenol/chloroform in phase lock tubes and precipitated by ethanol. Nucleic acid was digested with a combination of restriction enzymes (HindIII, BsrGI, XbaI and SspI) overnight at 37°C. For RNA/DNA/Protein immunoprecipitation, 5 μg of DNA was incubated with S9.6 antibody (5 μg) in binding buffer (10 mM NaPO4 pH 7.0, 140 mM NaCl, 0.05% Trixon X-100) overnight at 4 °C. Immunocomplexes were incubated with protein A/G magnetic beads (Thermo Fisher, USA) for 2 h at 4 °C. The beads were washed three times with binding buffer and the immunocomplexes were then eluted with elution buffer (50 mM Tris-HCl pH 8.0, 10 mM EDTA, 0.5% SDS) for 45 min at 55 °C. For qPCR, RNA/DNA/protein immunocomplexes were digested with Proteinase K (10 mg/ml) and re-extracted by phenol/chloroform in phase lock tubes and precipitated by ethanol. Quantitative real-time PCR was performed using SYBR® Green Master Mix (Bio-Rad, USA). Primers used for DRIP-qPCR were listed in Supplementary Table S1.

Animal experiments

A total of 48 12-week-old female BALB/c nude mice were purchased from the Beijing Huafukang BioScience Company. Specific pathogen-free grade facility was employed for mice raising and monitoring. To establish xenograft models of ovarian cancer, a total of 5×10^6 SKOV3 or A2780 cells infected with lentivirus containing shNC, shA1 or shA2 in 100 ml PBS were subcutaneously injected into the right flank of nude mice. After two weeks, all xenograft tumors were harvested, weighed, and fixed in

4% paraformaldehyde. All animal experiments were performed in compliance with the guidelines approved by the Ethics Committee of Medical School of Shenzhen University. Randomization and single blinding were used for measurement.

Statistical Analysis

Experiments were carried out in three to five technical and biological replicates, and statistical parameters including the sample size (*n*) and the significance analysis were specified in figure legends. GraphPad Prism 6 (La Jolla, CA, USA) was applied for statistical analysis. Two-tailed and unpaired Student's *t*-test were used to calculate significance in an interval of 95% confidence level, following normal distribution with different but similar SD values. Data were demonstrated as mean ± SEM. $P < 0.05$ was considered statistically significant.

Results

High ADAR1 expression correlates with poor PFS in Ovarian cancer.

To determine the status of ADAR1 in ovarian cancer clinical samples, we assessed ADAR1 mRNA expression in ovarian cancer tissues (n = 32) and normal ovarian surface epithelium tissues (n = 21) using quantitative reverse-transcription PCR (qRT-PCR). As shown in Fig.1a, ADAR1 mRNA expression was significantly upregulated in ovarian cancer tissue compared to normal tissue ($P < 0.001$). Consistent with the mRNA results, western blot analysis showed increased protein level of ADAR1 in ovarian cancer tissue (Fig.1b). To further verify the upregulation of ADAR1 in ovarian cancer tissue, we generated a tissue array containing 87 ovarian cancer tissues and 49 normal ovarian surface epithelium tissues for immunohistochemistry staining. A histological evaluation based on the histo-score (H-score) showed that strong ADAR1 staining (H-score ≥ 6) was found in 61 of 87 (70.1%) ovarian cancer tissues, while weak ADAR1 staining (H-score ≤ 6) was found in 41 of 49 (83.7%) normal tissues (Fig.1D). Progression free survival Kaplan–Meier analysis of published ovarian cancer microarray dataset (N = 1436) by "Kaplan–Meier Plotter" showed that high ADAR1 protein level strongly correlated with a poor outcome, whereas low ADAR1 protein level was associated with good progression free survival (Fig.1e, $P < 0.01$). Collectively, these results indicated that ADAR1 might play a critical role in the occurrence and progression of ovarian cancer.

Loss of ADAR1 inhibits ovarian cancer cell proliferation, clonogenicity and invasion.

Since ADAR1 upregulation was associated with poor prognosis in ovarian cancer, we attempted to explore the function of ADAR1 in ovarian cancer using *in vitro* cultured cell lines. Three ovarian cancer cell lines (SKOV3, A2780 and IGROV1) were used to construct stably knockdown cell lines by short hairpin mediated RNAs (shRNAs) of two independently targeted regions of ADAR1. Western blot was performed to examine the knockdown efficiency and the results showed that both ADAR1 shRNAs (shA1 and shA2) could significantly reduce ADAR1 protein levels in all three ovarian cancer cell lines compared with non-targeted scramble shRNA (Fig.2a). We then tested the effect of ADAR1 shRNAs on growth and

clonogenicity of ovarian cancer cells. Compared with scramble shRNA, both ADAR1 shRNAs significantly inhibited the proliferation of ovarian cancer cell lines, reflected by reduced cell numbers in ADAR1 shRNAs-treated cells (Fig.2b, P <0.01). Moreover, the ovarian cancer cell lines incubated with ADAR1 shRNAs showed smaller and fewer number of colonies than scramble shRNA-treated cells (Fig.2c, d). These results together indicated that ADAR1 played an important role in promoting ovarian cancer cell growth and clonogenicity. Lastly, we assessed cell migration using non-matrigel-coated transwell chambers and found that ADAR1 knockdown significantly repressed cell invasion (Fig. 2 e, f), which is consistent with previous report in lung cancer cells[2].

Loss of ADAR1 inhibits tumorigenesis of ovarian cancer cells *in vivo*.

Xenograft engraftment of ovarian cancer cells (SKOV3 and A2780) was generated to analyze the effect of ADAR1 on tumorigenesis *in vivo*. SKOV3 and A2780 cells with or without ADAR1 knockdown were implanted into the right flank of nude mice to generate xenografts. The tumors were collected for further analysis after 14 days. As shown in Fig. 3 a, b, ADAR1 shRNA-treated SKOV3 and A2780 cells showed significantly lower tumorigenicity compared with scramble shRNA-treated cells , reflected by smaller tumor volume and lower tumor weight . Further immunohistochemistry staining of the proliferation marker Ki67 indicated that the number of Ki-67 positive cells was significantly reduced in ADAR1 silence group, compared with control group (Fig. 3 c).

Loss of ADAR1 impairs ovarian cancer normal cell cycle.

To explore the mechanism underlying ADAR1's inhibitory effect on cell growth, we analyzed the changes of gene expression in SKOV3 cells treated with scramble shRNA or ADAR1 shRNA using RNA-seq and found that knockdown of ADAR1 led to 455 upregulated genes and 1044 downregulated genes ($p < 0.05$, fold change > 1.5) (Data not show). The KEGG pathway analysis results revealed that the differentially expressed genes were enriched in protein processing of endoplasmic reticulum, cell-cycle progression, splicing, mRNA surveillance pathway and p53 signaling pathway (Fig.4a), indicating a role of ADAR1 in cell cycle regulation. Moreover, heatmap analysis of cell cycle pathway revealed that the genes involved in the regulation of CMG complex (MCM2, MCM3, MCM5 and MCM6) and cell division cycle (CCNA2, CDC23, CDC25A and CDC25B) were repressed significantly (Fig.4b), and real-time PCR assay confirmed these RNA-seq findings (Fig.4c). To further demonstrate a role of ADAR1 in cell cycle regulation, BrdU-based cell cycle assay was performed in SKOV3 and A2780 cells. Results revealed that knockdown of ADAR1 led to a reduction in the number of S-phase cells, and an increase in the number of G1-phase cells (Fig. 4d, e), suggesting that silence of ADAR1 caused cell cycle arrest in G1/G0 phase. Taken together, these results indicated that ADAR1 played a crucial role in cell-cycle regulation of ovarian cancer cells.

Loss of ADAR1 causes DNA damage and ATR/Chk1 activation.

Loss of ADAR1 has been reported to trigger endogenous type 1 IFN response or PRK activation, thereby repressing cell growth and promoting cell apoptosis in several types of cancer cell lines [17, 25]. Surprisingly, we did not observe the activation of endogenous type 1 IFN pathway and PKR when ADAR1

was knocked down (FigS. 1 a-d), indicating that ADAR1 silence-induced cell cycle arrest was independent of type 1 IFN or PKR pathway in ovarian cancer cells. Since the RNA-seq results had shown that p53 and cell cycle pathway were affected by loss of ADAR1, we next assessed DNA damage status that is critical for cell cycle checkpoint and p53 pathway activation. As shown in Fig. 5 a-b, the number of γH2AX foci (a biomarker for DNA damage) was increased when ADAR1 was knocked down in both SKOV3 and A2780 cells.

Previous studies reported that double-strand DNA break could cause the phosphorylation of both Chk1, a substrate of the ATR checkpoint kinase, and Chk2, a substrate of the ATM checkpoint kinase, while single-strand DNA break could only activate Chk1 [11, 37]. To further explore type of DNA damage caused by ADAR1 silence in ovarian cancer cells, we detected the phosphorylation status of Chk1, Chk2, ATR, ATM and RPA32. As shown in Fig. 5c, loss of ADAR1 only increased the phosphorylation of Chk1, ATR and RPA32, but had no effect on the phosphorylation of Chk2 and ATM (Fig.5 c). These results indicated that ADAR1 silence induced single-strand but not double-strand DNA breaks in ovarian cancer cells.

R loop-driven ATR Pathway is involved in DNA damage caused by loss of ADAR1.

Previous studies have demonstrated that abnormal accumulation of R loops can cause activation of ATR-Chk1, but not ATM-Chk2 pathway[11, 18, 27]. Hence, we speculated that cell cycle arrest induced by ADAR1 silence might result from R-loops accumulation. To confirm this, we used S9.6 antibody to detect the RNA–DNA hybrid component of R-loops. As shown in Fig. 6 a, b, knockdown of ADAR1 caused a significant increase in RNA–DNA hybrids fluorescent in SKOV3 cells, indicating that ADAR1 silence induced intense R-loop accumulation. To further determine whether R-loops accumulation occurred to specific genes, we performed DNA/RNA immunoprecipitation (DRIP) analysis for two well-studied gene locus (β-actin and rpl13a locus) by real-time PCR[8]. Primers for DRIP-qPCR were designed for different regions of the genes, including transcriptional start region, gene body (intron and exon), and transcription termination region (Fig.6 c). Results revealed that knockdown of ADAR1 significantly increased DNA/RNA hybrids in nearly all regions of β-actin and rpl13a gene (Fig. 6 d). Lastly, we conducted rescue experiments by overexpressing RNase H1 in ADAR1 shRNA-treated ovarian cancer cells , as RNase H1 is a well-studied enzyme that could effectively eliminate intracellular R loop [11]. As expected, RNase H1 overexpression significantly reduced the levels of pChk1 and γH2AX in ADAR1-silienced ovarian cancer cells (Fig. 6 e f). Together, these results indicated that loss of ADAR1 could cause R loop accumulation and thus activated ATR/Chk1 cell cycle checkpoint to repress cell growth and tumorigenesis.

ADAR1 interacts with DHX9 to regulate R-Loop formation.

We next investigated the mechanism by which ADAR1 regulates the level of R-loop in ovarian cancer. Firstly, we conducted DNA/RNA-IP experiments by using S9.6 to pull down DNA/RNA hybrid-protein complex. We found that both ADAR1 and DHX9, a well-known ADAR1 interaction protein, were directly interacted with R-loop complex (Fig. 7 a), suggesting that ADAR1 might directly regulate R Loop formation. This finding was consistent with two recent reports in which DHX9 has been reported to

unwind nascent RNA and facilitate nascent RNA to invade duplex DNA to form R-loop[8, 13]. Then Co-IP was performed to confirmed previous report of interaction between ADAR1 and DHX9 (Fig. 7 b). Of note, RNase A treatment had no effect on the interaction, suggesting ADAR1 physical interact with DHX9 independent on RNA. Lastly, to further clarify the role of DHX9, we knocked down DHX9 using siRNA in ADAR1 silenced SKOV3 cells, and found that knockdown of DHX9 could partially improve cell growth and its response to DNA damage in ADAR1-silenced cells (Fig. 7 c d). Taken together, these results indicated that ADAR1 was directly involved in DNA/RNA hybrid-protein complex, and interacted with DHX9 to regulate R-loop formation.

RNA editing regulates R-Loop formation.

To further explore the mechanism of ADAR1 underlying R-loop regulation, we tested whether RNA adenosine deaminase domain was essential for R-loop regulation. We constructed an ADAR1 expressing vector ADAR1^{E912A} that contained an inactive deaminase domain with E912A mutation (Glu912→Ala912). We overexpressed ADAR1^{E912A} or wild-type ADAR1 in ADAR1-silenced SKOV3 cells. Of note, we found that overexpression of wild-type ADAR1, but not ADAR1^{E912A}, could rescue cell growth and DNA damage response in ADAR1-silenced SKOV3 cells (Fig. 8a, b). Similarly, R-loop level was also only rescued by the overexpression of wild-type ADAR1, but not ADAR1^{E912A} (Fig. 8 c). Taken together, these results indicated that normal RNA editing was critical for preventing R-loop formation.

Discussion

ADAR1 has been reported to promote tumor growth and metastasis as an oncogene in several types of human cancers[3, 4, 10, 19-21, 23, 29]. In this study, we demonstrated an important role in the tumorigenesis and progression in ovarian cancer. The major findings are as follows: 1) ADAR1 was highly expressed in ovarian cancer tissue and was negatively correlated with progression free survival in ovarian cancer patients; 2) knockdown of ADAR1 suppressed ovarian cancer cell growth and colony formation *in vitro* and inhibited ovarian cancer cell tumorigenesis *in vivo*; 3) cell cycle and transcriptome profile analysis demonstrated that knockdown of ADAR1 induced ovarian cancer cell cycle arrest at G1/G0 stage; 4) loss of ADAR1 disrupted its interaction with DHX9 and caused R-loop abnormal accumulation, thereby contributing to single stand DNA break and ATR pathway activation..

ADAR1 has been shown to act on RNA editing to promote cancer cell survival, growth and migration in different types of cancer cells through multiple molecular functions. For example, in lung cancer, loss of ADAR1 represses cell growth through editing miR-381[3] and inhibits cell migration through editing mRNA of FAK[2]. In chronic myeloid leukemia, silence of ADAR1 inhibits leukemia stem cell self-renewal through impairing let-7 miRNA biogenesis[42] or causes cell cycle arrest through repressing miR-26a maturation[21]. Recently, it has been reported that deletion of ADAR1 leads to lethal phenotype in cancer cell lines with strong IFN-stimulated gene (ISG) signature through activation of PKR pathway [17, 25]. Here, the two ovarian cancer cell lines SKOV3 and A2780 used in this study were negative for ISG signature, as their

threshold cycles of IFN-stimulated genes were both more than 35 in real time PCR. Probably due to lack of ISG signature, ADAR1 silence did not elevate PKR activation in SKOV3 and A2780 cells, when ADAR1 was silenced. Together, in ovarian cancer cell lines without ISG signature, indicating that ADAR1 may exert its action in a PKR pathway-independent was in cells without ISG signature.

DNA damage response (DDR) is one of the most important factors leading to p53 activation and cell cycle arrest. When DNA damage occurs, DNA damage-sensing proteins and intermediary proteins will accumulate at the site of DNA damage and activate the conductive protein ATM or ATR[26]. Previous studies have shown that double-stranded DNA breaks can directly activate ATM/Chk2 pathway, and also recruit and activate ATR/Chk1 pathway by the single-stranded DNA generated during the repair of double-stranded DNA breaks. However, single-stranded DNA damage can only recruit and activate ATR/Chk1 pathway[37]. Our results showed that ADAR1 knockdown caused increase of phosphorylation of Chk1 and ATR, but not phosphorylation of Chk2 and ATM, indicating that single strand DNA damage was generated by ADAR1 knockdown in ovarian cancer cells. Furthermore, we also showed that knockdown of ADAR1 caused a global R-loop abnormal accumulation and overexpression of RNase H1 could rescue R-loop accumulation and DNA damage, suggesting that R-loop accumulation plays a key role for DNA damage and cell cycle arrest in ovarian cancer cells.

R-loop is a special nucleic acid structure formed during transcription process, which is consisted of two antiparallel DNA strands plus one RNA strand. In this structure, the nascent RNA is base-paired to one of the DNA strands to form DNA/RNA hybrids, while the other DNA strand is unpaired. R-loop has been reported to play an important role in gene transcription[38], immunoglobulin class switch recombination[41] and chromatin epigenetic modification[33]. Abnormal R-loop accumulation can lead to replication stress and single-stranded DNA damage[18, 27]. For response to replication stress and DNA damage, cells can activate ATR pathway that mediates the activation of DNA repair pathways and stabilization of replication forks[6, 7]. In ovarian cancer, increased replication stress and DNA damage are prevalent, and inhibition of ATR may represent an effective strategy for ovarian cancer therapy. Recently, a phase 2 clinical trial has shown that administration of the ATR inhibitor berzosertib with gemcitabine increased progression-free survival in patients with high-grade ovarian cancer compared with gemcitabine alone[22], suggesting that ATR inhibitor is beneficial for ovarian cancer therapy. Additionally, myeloid leukemia cells with R-loop accumulation induced by splicing factor disorder has been reported to be more sensitive to ATR inhibitors[27]. Hence, it's a good strategy to explore combination ATR inhibitor and ADAR1 inhibitor for ovarian cancer treatment in future studies. Luckily, high-throughput screen of RNA editing inhibitors using a small molecule library has been performed, which could greatly accelerate ADAR1 targeted anti-tumor therapy[16].

DHX9 has been reported to interact with ADAR1 to regulate A to I editing[19] and protect genome from short interspersed nuclear element (SINE) insertions[1]. Additionally, DHX9 has been reported to unwind nascent double-stranded RNA during co-transcriptional process, and is implicated in the formation of R-loop[8, 13]. Here, we also demonstrated that ADAR1 interacted with DHX9 to directly contribute to the formation of R-

Loop complex, which was further supported by our data that silence of DHX9 partly rescued R-loop accumulation resulting from ADAR1 knockdown.

Previous studies have shown that A to I RNA editing by ADAR1 induces various functional changes, such as direct changes in the protein sequence by editing coding region of mRNA[2, 14], changes in miRNA targets by editing pri-miRNA and pre-miRNA target sites[21, 42], altered immunogenicity of endogenous RNA by editing double strand RNA[12, 24], and enhanced mRNA stability by editing 5'UTR region of mRNA[32, 35]. Here, our data that only wild-type ADAR1 but not ADAR1^{E912A} could rescue R-loop accumulation and DNA damage suggest that A to I RNA editing is crucial for maintaining R-loop level. However, a global view of RNA editing function on R-loop is still lacking. In future studies, genome-wide methods, including Nascent RNA sequencing and DRIP-Seq should be performed to reveal the accurate relationship between RNA editing and R-loop.

Conclusion

In summary, our work has demonstrated ADAR1 as a pivotal oncogene in ovarian cancer cells. ADAR silence induces cell cycle arrest and single strand DNA damage by activating R-loop-driven ATR Pathway. Mechanistically, without ADAR1, low edited double-stranded nascent RNA is unwound by DHX9 to generate free single strand RNA, and then annealing with template DNA strand to generate a strong DNA–RNA hybrid with perfect matched. The novel ADAR1/R-loop/ATR axis is critical for ovarian cancer progression and a potential target for ovarian cancer therapy.

Abbreviations

ADAR1: adenosine deaminases acting on RNA 1

IHC: Immunohistochemistry

PFS: Progress Free Survival

shNC: Short hairpin RNA for targeting non-coding sequence

shA1: Short hairpin RNA 1 for targeting ADAR1

shA2: Short hairpin RNA 2 for targeting ADAR1

RNA-Seq: RNA sequencing

KEGG: Kyoto Encyclopedia of Genes and Genomes

BrdU: 5-Bromo-2-deoxyUridine

D/RIP: DNA/RNA Immunoprecipitation

Declarations

Ethics approval and consent to participate

Procedures for the collection of human samples and their usage for tissue arrays were approved by the Ethical Committee of the Army Medical University (Chongqing, China). All patients signed an informed consent for participating in this study. All animal experiments were performed in compliance with the guidelines approved by the Ethics Committee of Medical School of Shenzhen University.

Consent for publication

The content of this manuscript has not been published or submitted for publication elsewhere. All the authors listed have approved the manuscript that is enclosed. They have read and understood your journal’s policies, and they believe that neither the manuscript nor the study violates any of these.

Availability of data and materials

The datasets used and/or analyzed during the current study are available from the corresponding author on reasonable request.

Competing interests

The authors of this article declare that they have no known competing financial interests or personal relationships that could have appeared to influence the work reported in this paper.

Funding

This work was supported by funds from the National Natural Sciences Foundation of China (81801639 to Hanwei Cui), Shenzhen Science and Technology Commission (JCYJ20170817172241688 and JCYJ20170817172150505 to Xiufeng Ye, JCYJ20170413104646428 to Wenlan Liu), and China Postdoctoral Science Foundation Grant (2019M663105 to Hanwei Cui).

Authors' contributions

Dr. Hanwei Cui and Dr. Qi Yi contributed equally to this study.

HWC and WLL designed the study and preparing the first draft of the manuscript. QY and MT performed molecular biology experiments. YTL, WCS and JH carried out cell culture experiments and fed the animal models., ZQ, JH and ZYY collected clinical samples. XFY, WLL and JYG instructed and finalized the study. All authors read and approved the final manuscript.

Acknowledgements

Thanks for gift of RNase H1 overexpression plasmid from professor Liang Chen of Wuhan University.

References

1 Aktas T, Avsar Ilik I, Maticzka D, Bhardwaj V, Pessoa Rodrigues C, Mittler G *et al*. DHX9 suppresses RNA processing defects originating from the Alu invasion of the human genome. Nature 2017; 544: 115-119.

2 Amin EM, Liu Y, Deng S, Tan KS, Chudgar N, Mayo MW *et al*. The RNA-editing enzyme ADAR promotes lung adenocarcinoma migration and invasion by stabilizing FAK. Sci Signal 2017; 10.

3 Anadon C, Guil S, Simo-Riudalbas L, Moutinho C, Setien F, Martinez-Cardus A *et al*. Gene amplification-associated overexpression of the RNA editing enzyme ADAR1 enhances human lung tumorigenesis. Oncogene 2016; 35: 4407-4413.

4 Bhate A, Sun T, Li JB. ADAR1: A New Target for Immuno-oncology Therapy. Mol Cell 2019; 73: 866-868.

5 Bowtell DD, Bohm S, Ahmed AA, Aspuria PJ, Bast RC, Jr., Beral V *et al*. Rethinking ovarian cancer II: reducing mortality from high-grade serous ovarian cancer. Nat Rev Cancer 2015; 15: 668-679.

6 Cancer Genome Atlas Research N. Integrated genomic analyses of ovarian carcinoma. Nature 2011; 474: 609-615.

7 Ceccaldi R, O'Connor KW, Mouw KW, Li AY, Matulonis UA, D'Andrea AD *et al*. A unique subset of epithelial ovarian cancers with platinum sensitivity and PARP inhibitor resistance. Cancer Res 2015; 75: 628-634.

8 Chakraborty P, Huang JTJ, Hiom K. DHX9 helicase promotes R-loop formation in cells with impaired RNA splicing. Nat Commun 2018; 9: 4346.

9 Chan TH, Lin CH, Qi L, Fei J, Li Y, Yong KJ *et al*. A disrupted RNA editing balance mediated by ADARs (Adenosine DeAminases that act on RNA) in human hepatocellular carcinoma. Gut 2014; 63: 832-843.

10 Chan TH, Qamra A, Tan KT, Guo J, Yang H, Qi L *et al*. ADAR-Mediated RNA Editing Predicts Progression and Prognosis of Gastric Cancer. Gastroenterology 2016; 151: 637-650 e610.

11 Chen L, Chen JY, Huang YJ, Gu Y, Qiu J, Qian H *et al*. The Augmented R-Loop Is a Unifying Mechanism for Myelodysplastic Syndromes Induced by High-Risk Splicing Factor Mutations. Mol Cell 2018; 69: 412-425 e416.

12 Chung H, Calis JJA, Wu X, Sun T, Yu Y, Sarbanes SL *et al*. Human ADAR1 Prevents Endogenous RNA from Triggering Translational Shutdown. Cell 2018; 172: 811-824 e814.

13 Cristini A, Groh M, Kristiansen MS, Gromak N. RNA/DNA Hybrid Interactome Identifies DXH9 as a Molecular Player in Transcriptional Termination and R-Loop-Associated DNA Damage. Cell Rep 2018; 23: 1891-1905.

14 Forni D, Mozzi A, Pontremoli C, Vertemara J, Pozzoli U, Biasin M *et al*. Diverse selective regimes shape genetic diversity at ADAR genes and at their coding targets. RNA Biol 2015; 12: 149-161.

15 Fritzell K, Xu LD, Lagergren J, Ohman M. ADARs and editing: The role of A-to-I RNA modification in cancer progression. Semin Cell Dev Biol 2018; 79: 123-130.

16 Fritzell K, Xu LD, Otrocka M, Andreasson C, Ohman M. Sensitive ADAR editing reporter in cancer cells enables high-throughput screening of small molecule libraries. Nucleic Acids Res 2019; 47: e22.

17 Gannon HS, Zou T, Kiessling MK, Gao GF, Cai D, Choi PS *et al*. Identification of ADAR1 adenosine deaminase dependency in a subset of cancer cells. Nat Commun 2018; 9: 5450.

18 Hamperl S, Bocek MJ, Saldivar JC, Swigut T, Cimprich KA. Transcription-Replication Conflict Orientation Modulates R-Loop Levels and Activates Distinct DNA Damage Responses. Cell 2017; 170: 774-786 e719.

19 Hong H, An O, Chan THM, Ng VHE, Kwok HS, Lin JS *et al*. Bidirectional regulation of adenosine-to-inosine (A-to-I) RNA editing by DEAH box helicase 9 (DHX9) in cancer. Nucleic Acids Res 2018; 46: 7953-7969.

20 Ishizuka JJ, Manguso RT, Cheruiyot CK, Bi K, Panda A, Iracheta-Vellve A *et al*. Loss of ADAR1 in tumours overcomes resistance to immune checkpoint blockade. Nature 2019; 565: 43-48.

21 Jiang Q, Isquith J, Zipeto MA, Diep RH, Pham J, Delos Santos N *et al*. Hyper-Editing of Cell-Cycle Regulatory and Tumor Suppressor RNA Promotes Malignant Progenitor Propagation. Cancer Cell 2019; 35: 81-94 e87.

22 Konstantinopoulos PA, Cheng SC, Wahner Hendrickson AE, Penson RT, Schumer ST, Doyle LA *et al*. Berzosertib plus gemcitabine versus gemcitabine alone in platinum-resistant high-grade serous ovarian cancer: a multicentre, open-label, randomised, phase 2 trial. Lancet Oncol 2020; 21: 957-968.

23 Li Y, Banerjee S, Goldstein SA, Dong B, Gaughan C, Rath S *et al*. Ribonuclease L mediates the cell-lethal phenotype of double-stranded RNA editing enzyme ADAR1 deficiency in a human cell line. Elife 2017; 6.

24 Liddicoat BJ, Piskol R, Chalk AM, Ramaswami G, Higuchi M, Hartner JC *et al*. RNA editing by ADAR1 prevents MDA5 sensing of endogenous dsRNA as nonself. Science 2015; 349: 1115-1120.

25 Liu H, Golji J, Brodeur LK, Chung FS, Chen JT, deBeaumont RS *et al*. Tumor-derived IFN triggers chronic pathway agonism and sensitivity to ADAR loss. Nat Med 2019; 25: 95-102.

26 Marechal A, Zou L. DNA damage sensing by the ATM and ATR kinases. Cold Spring Harb Perspect Biol 2013; 5.

27 Nguyen HD, Leong WY, Li W, Reddy PNG, Sullivan JD, Walter MJ *et al*. Spliceosome Mutations Induce R Loop-Associated Sensitivity to ATR Inhibition in Myelodysplastic Syndromes. Cancer Res 2018; 78: 5363-5374.

28 Ota H, Sakurai M, Gupta R, Valente L, Wulff BE, Ariyoshi K *et al*. ADAR1 forms a complex with Dicer to promote microRNA processing and RNA-induced gene silencing. Cell 2013; 153: 575-589.

29 Qi L, Song Y, Chan THM, Yang H, Lin CH, Tay DJT *et al*. An RNA editing/dsRNA binding-independent gene regulatory mechanism of ADARs and its clinical implication in cancer. Nucleic Acids Res 2017; 45: 10436-10451.

30 Qin YR, Qiao JJ, Chan TH, Zhu YH, Li FF, Liu H *et al*. Adenosine-to-inosine RNA editing mediated by ADARs in esophageal squamous cell carcinoma. Cancer Res 2014; 74: 840-851.

31 Rossetti C, Picardi E, Ye M, Camilli G, D'Erchia AM, Cucina L *et al*. RNA editing signature during myeloid leukemia cell differentiation. Leukemia 2017; 31: 2824-2832.

32 Sakurai M, Shiromoto Y, Ota H, Song C, Kossenkov AV, Wickramasinghe J *et al*. ADAR1 controls apoptosis of stressed cells by inhibiting Staufen1-mediated mRNA decay. Nat Struct Mol Biol 2017; 24: 534-543.

33 Sanz LA, Hartono SR, Lim YW, Steyaert S, Rajpurkar A, Ginno PA *et al*. Prevalent, Dynamic, and Conserved R-Loop Structures Associate with Specific Epigenomic Signatures in Mammals. Mol Cell 2016; 63: 167-178.

34 Sharpnack MF, Chen B, Aran D, Kosti I, Sharpnack DD, Carbone DP *et al*. Global Transcriptome Analysis of RNA Abundance Regulation by ADAR in Lung Adenocarcinoma. EBioMedicine 2018; 27: 167-175.

35 Shen Q, Zhang Q, Shi Y, Shi Q, Jiang Y, Gu Y *et al*. Tet2 promotes pathogen infection-induced myelopoiesis through mRNA oxidation. Nature 2018; 554: 123-127.

36 Siegel RL, Miller KD, Jemal A. Cancer statistics, 2018. CA Cancer J Clin 2018; 68: 7-30.

37 Smith J, Tho LM, Xu N, Gillespie DA. The ATM-Chk2 and ATR-Chk1 pathways in DNA damage signaling and cancer. Adv Cancer Res 2010; 108: 73-112.

38 Sun Q, Csorba T, Skourti-Stathaki K, Proudfoot NJ, Dean C. R-loop stabilization represses antisense transcription at the Arabidopsis FLC locus. Science 2013; 340: 619-621.

39 Tan MH, Li Q, Shanmugam R, Piskol R, Kohler J, Young AN *et al*. Dynamic landscape and regulation of RNA editing in mammals. Nature 2017; 550: 249-254.

40 Wang C, Zou J, Ma X, Wang E, Peng G. Mechanisms and implications of ADAR-mediated RNA editing in cancer. Cancer Lett 2017; 411: 27-34.

41 Yu K, Chedin F, Hsieh CL, Wilson TE, Lieber MR. R-loops at immunoglobulin class switch regions in the chromosomes of stimulated B cells. Nat Immunol 2003; 4: 442-451.

42 Zipeto MA, Court AC, Sadarangani A, Delos Santos NP, Balaian L, Chun HJ *et al*. ADAR1 Activation Drives Leukemia Stem Cell Self-Renewal by Impairing Let-7 Biogenesis. Cell Stem Cell 2016; 19: 177-191.

Figures

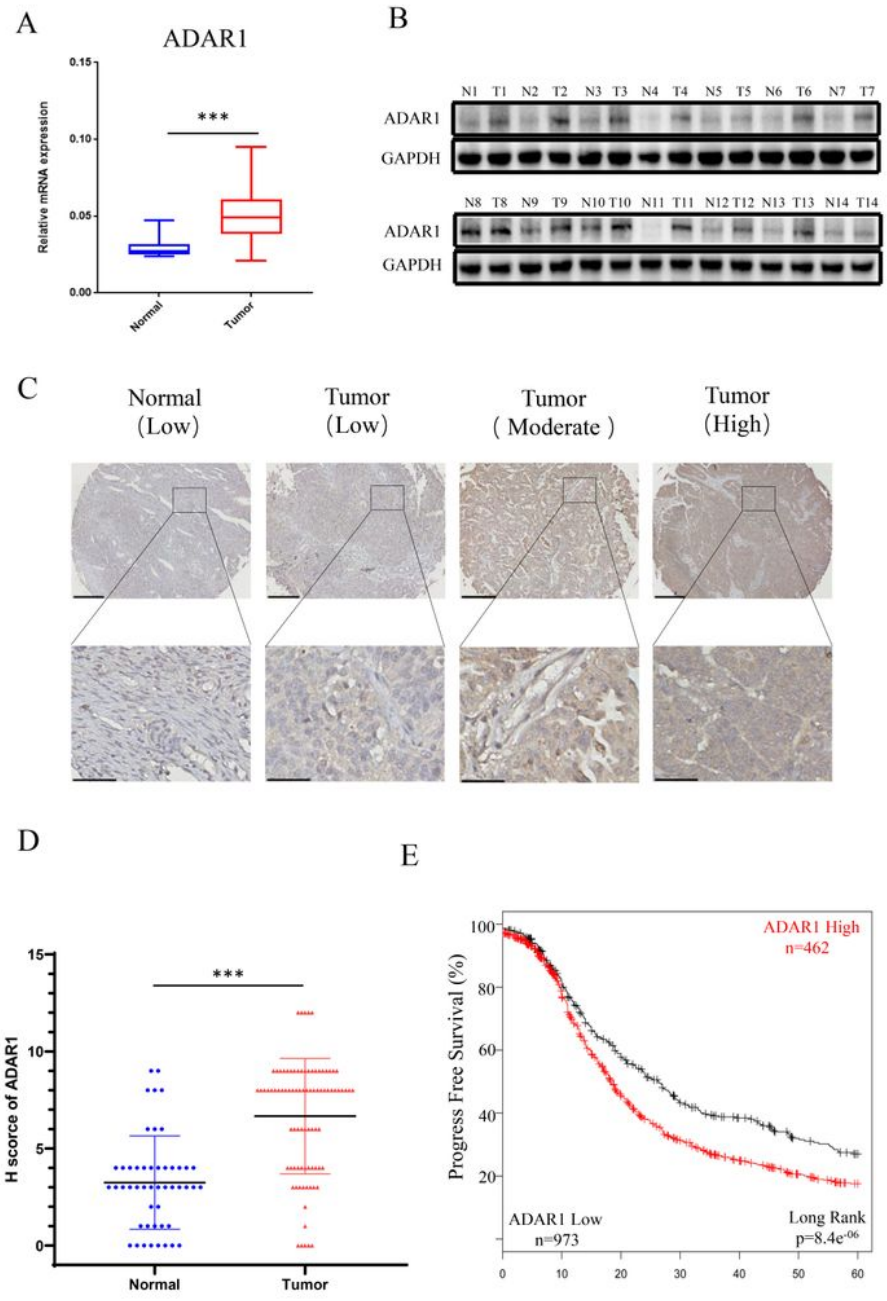

Figure 1

High ADAR1 expression correlates with poor PFS in Ovarian cancer. (A) mRNA levels of ADAR1 in ovarian cancer tissues and normal ovarian surface epithelium tissues were quantified by quantitative reverse-transcription PCR. ADAR1 expression was normalized by GAPDH expression and each noncancerous ovarian surface epithelium tissues were used as a control. Data were shown as mean ± SD. (***, P<0.001 **, P<0.01 *, P<0.05) (B) Protein levels of ADAR1 in ovarian cancer tissues (T) and normal ovarian surface

epithelium tissues (N) were determined by western blot. GAPDH expression served as endogenous reference. (C) Assessment of ADAR1 protein expression in ovarian cancer tissues and normal ovarian surface epithelium tissues by immunohistochemical analysis. The representative microphotographs showed high, moderate and low staining of ADAR1 in tissue array. Upper scale bar, 200 μm; lower scale bar, 50 μm. (D) Quantification analysis of ADAR1 protein stain of (C) by H scores Data were shown as mean ± SD. (***, P<0.001 **, P<0.01 *, P<0.05). (E) Kaplan-Meier curve of progression-free survival of ovarian cancer patients according to the expression level of ADAR1 protein in ovarian cancer tissues (ADAR1 High-expression, n = 462 and ADAR1 Low-expression, n = 973) from TCGA database.

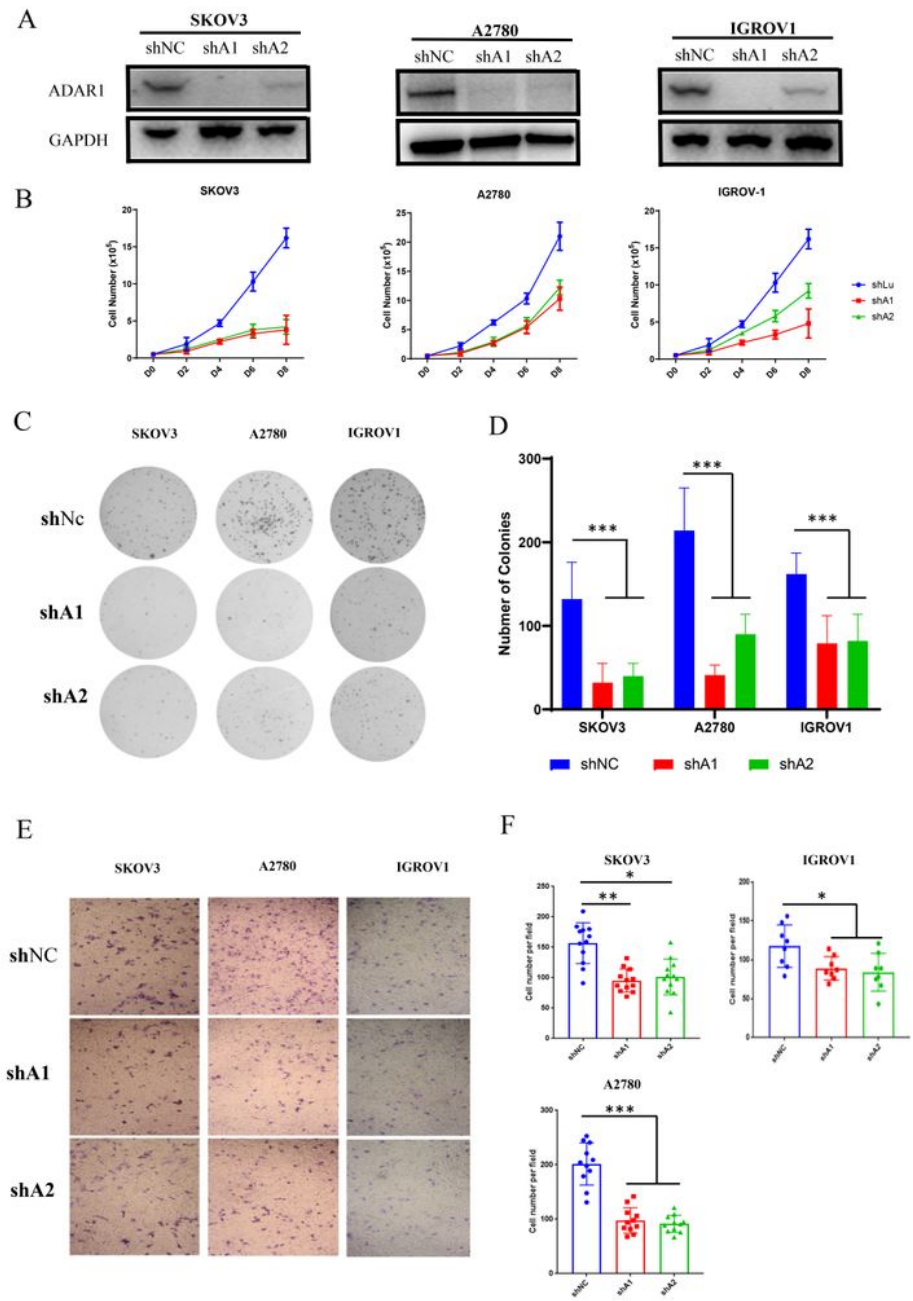

Figure 2

ADAR1 deficiency inhibits ovarian cancer cell proliferation, clonogenicity and invasion in vitro. (A) Protein levels of ADAR1 were determined in three ovarian cancer cell lines (SKOV3, A2780 and IGROV1) by western blot. shA1 means shRNA 1 targeting ADAR1; shA2 means shRNA 2 targeting ADAR1. (B) Cell growth curve of SKOV3, A2780 and IGROV1 with or without ADAR1 silence. All data were shown as mean ± SD from four independent experiments. (C) The representative microphotographs showed the colony

formation of SKOV3, A2780 and IGROV1 cells with or without ADAR1 silence. Representative photographs showed the colony formation of SKOV3, A2780 and IGROV1. (D) The number of colonies in (C) were shown in histograms. All data were shown as mean ± SD from three independent experiments (***, P<0.001 **, P<0.01 *, P<0.05). (E) The representative microphotographs showed the migration of SKOV3, A2780 and IGROV1 cells with or without ADAR1 silence. The migrated cell numbers of (E) were shown in histograms. All data were shown as means ± SD from three independent experiments (***, P<0.001 **, P<0.01 *, P<0.05).

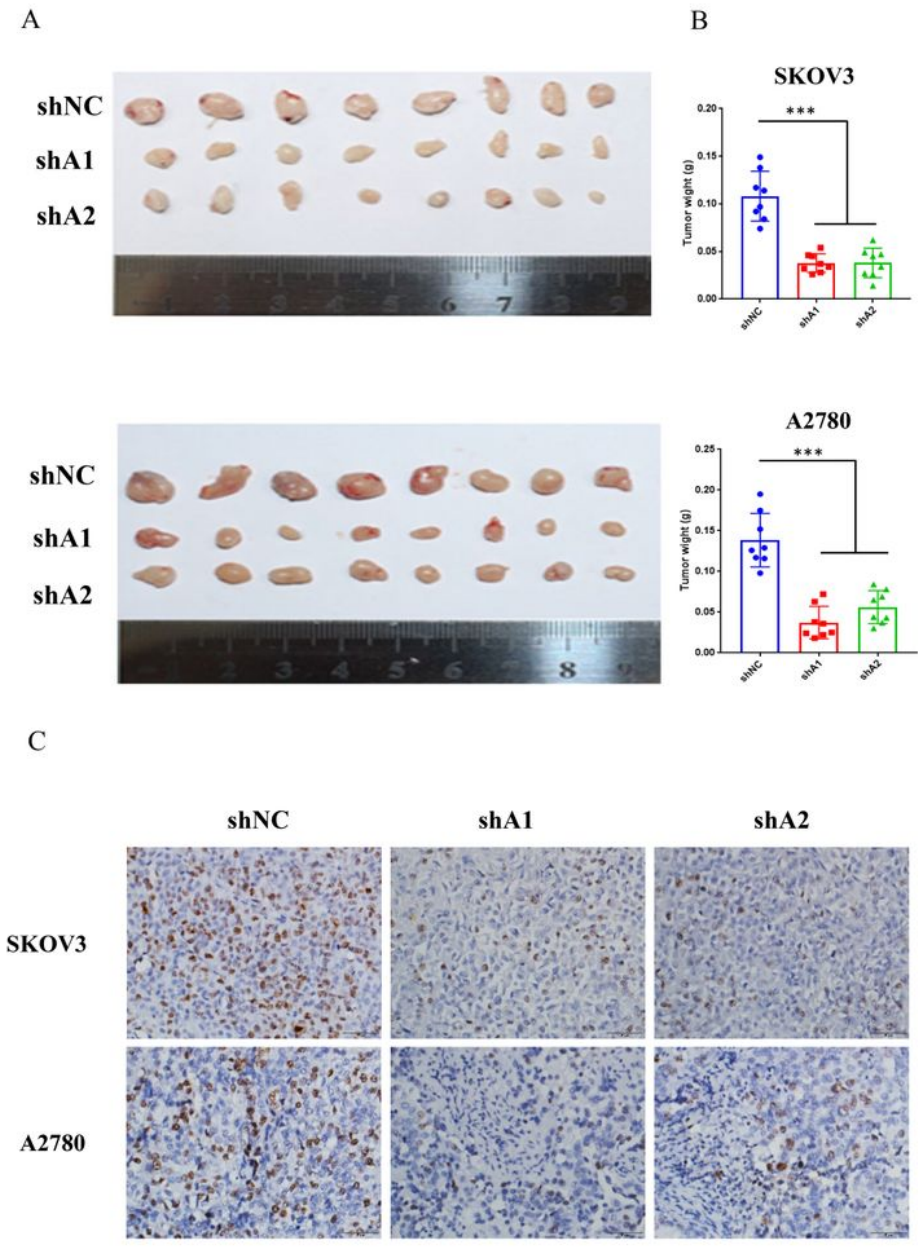

Figure 3

ADAR1 deficiency represses ovarian cancer tumorigenesis in vivo. (A)SKOV3 and A2780 cells with or without ADAR1 silence were subcutaneously inoculated in BALB/c nude mice. Two weeks later, xenograft tumors were harvested and displayed. (B)The weight of xenograft tumors was measured and shown in histograms. Data were shown as means ± S.D. (***, P<0.001 **, P<0.01 *, P<0.05). (C) Immunohistochemical analysis of Ki67 was performed on xenografts tumors. Representative images were shown. Scale bar, 50 μm.

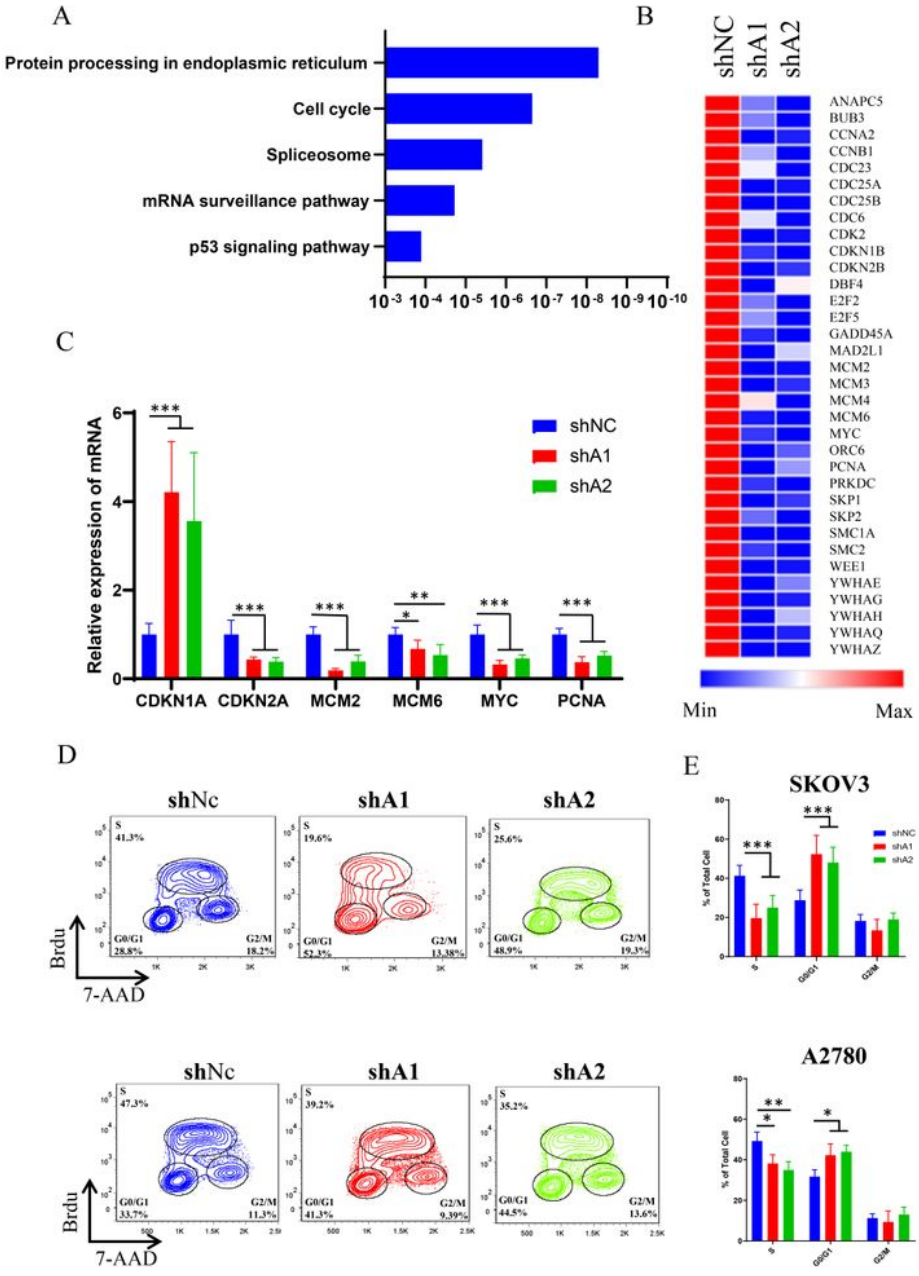

Figure 4

ADAR1 deficiency causes ovarian cancer cell cycle arrest. (A) KEGG analysis of differentially expressed genes when ADAR1 deficiency. (B) Heatmap of differentially expressed genes in cell cycle pathway when ADAR1 deficiency. (C) mRNA levels of genes in cell cycle pathway quantified by quantitative reverse-transcription PCR. (D) The representative scatter plot graph showed the cell cycle of SKOV3 and A2780 cells with or without ADAR1 silence. Cell cycle analysis was performed on the scatter plot graph. All data were shown as mean ± SD from three independent experiments (***, P<0.001 **, P<0.01 *, P<0.05).

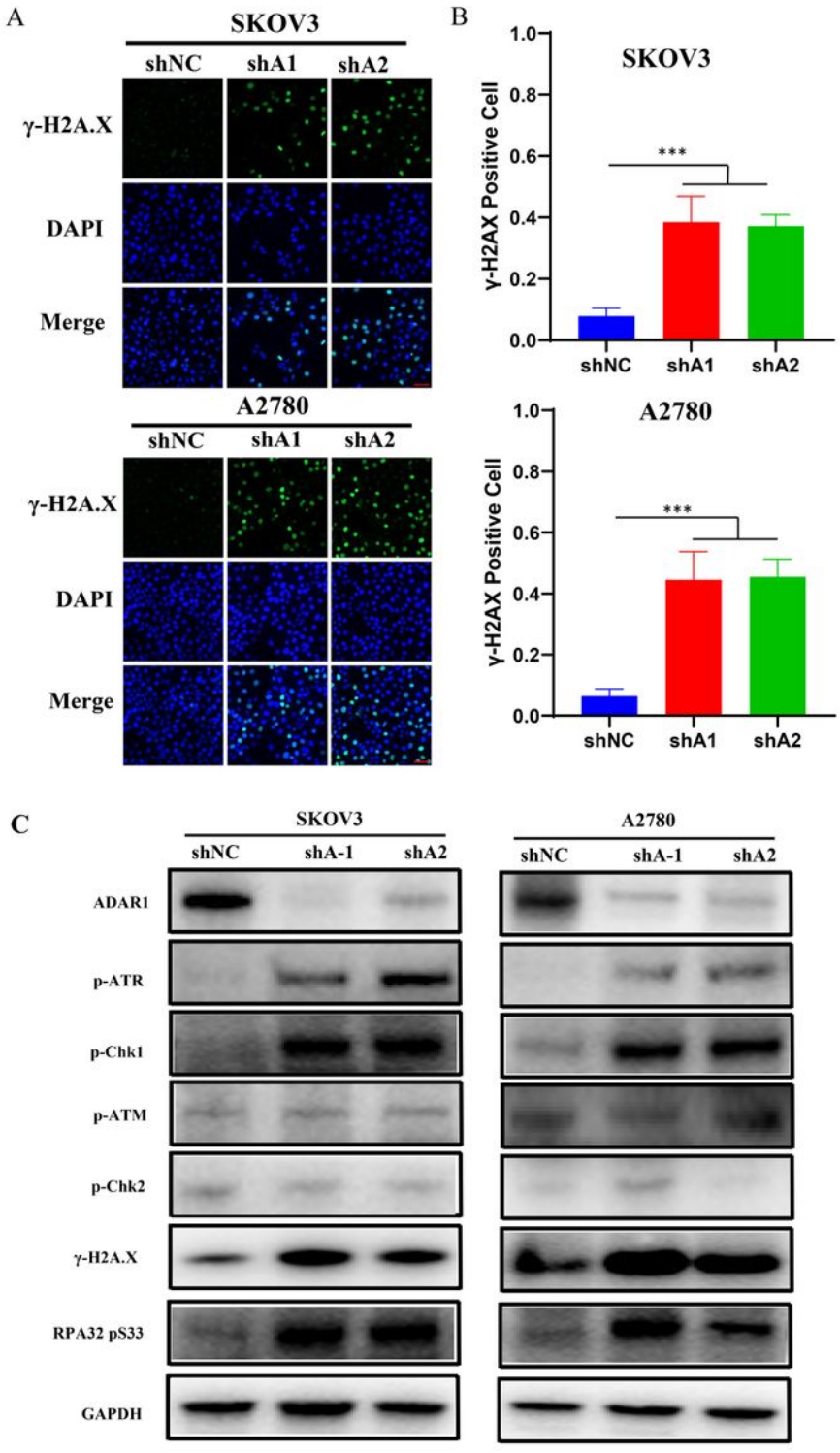

Figure 5

ADAR1 deficiency cause DNA damage and ATR/Chk1 activation. (A) The representative microphotographs showed Immunostaining of γH2AX foci in SKOV3 and A2780 cells with or without ADAR1 silence. Scale bar, 50 μm. (B) Quantification analysis of percentage of γH2AX foci positive cell in (A). All data were shown as mean ± SD. (***, P<0.001 **, P<0.01 *, P<0.05). (C) Protein levels of DNA Damage Response pathway (phosphorylation of ATM/Chk1, phosphorylation of ATR/Chk2, phosphorylation of RPA32 and γH2AX) were measured in SKOV3 and A2780 cells with or without ADAR1 silence by western blot.

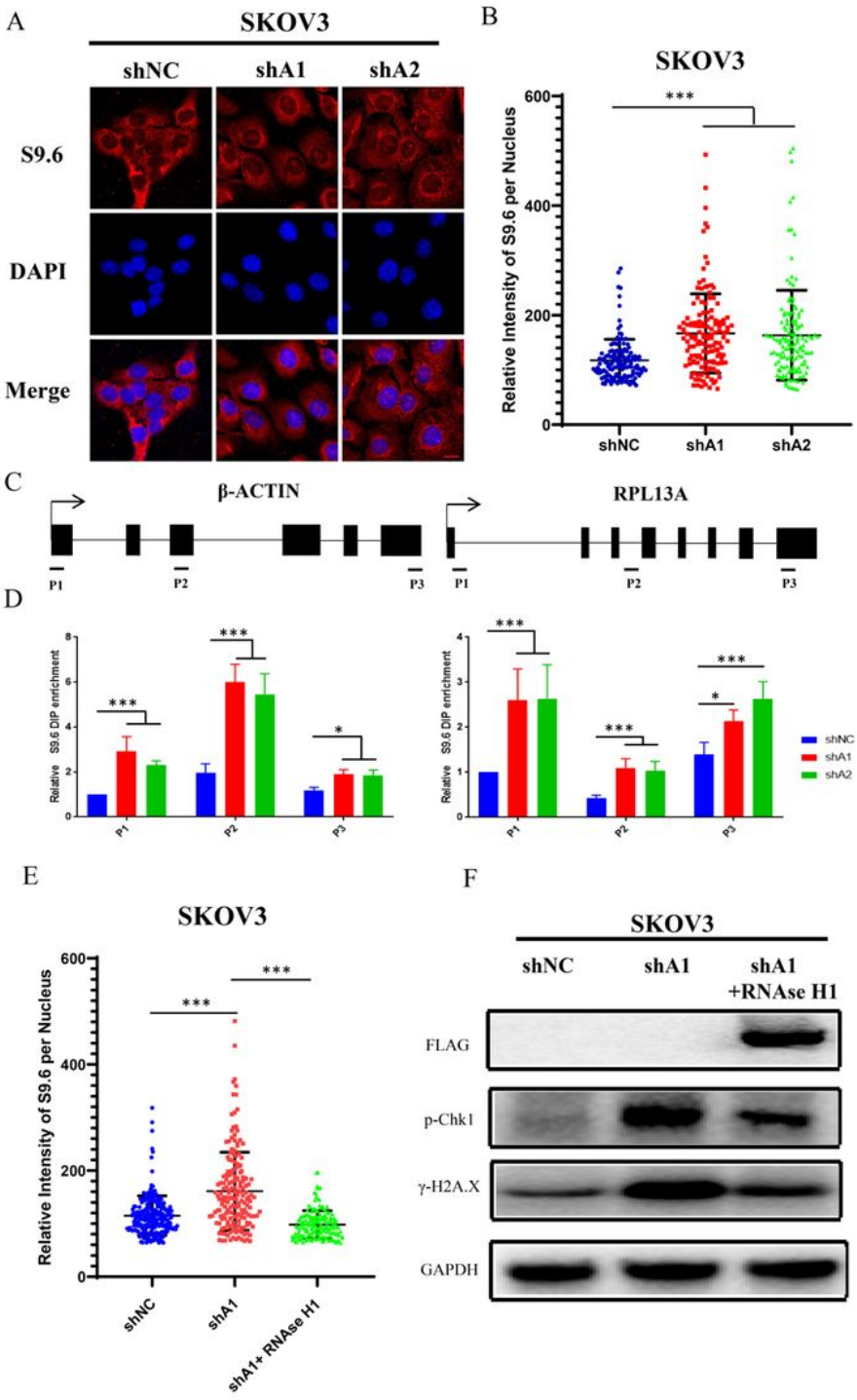

Figure 6

R loop is involved in ATR/Chk1 pathway activation by ADAR1 deficiency. (A) The representative microphotographs showed immunostaining of DNA/RNA hybrid (S9.6 antibody) in SKOV3 with or without ADAR1 silence. Scale bar, 20 μm. (B) Quantification of mean intensity of DNA/RNA hybrid in (A). All data were shown as mean ± SD in n > 90 cells. (***, P<0.001 **, P<0.01 *, P<0.05). (C) Diagram of the β-actin and RPL13A locus depicting relative position of primer pairs used for DRIP–qPCR. Exons are

depicted as black boxes. (D) DRIP–qPCR was performed using primers to the indicated regions of the β-actin and RPL13A in SKOV3 cells with or without ADAR1 silence. (***, P<0.001 **, P<0.01 *, P<0.05). (E) Quantification of mean intensity of DNA/RNA hybrid in SKOV3 with scramble shRNA and SKOV3 with ADAR1shRNA. SKOV3 with ADAR1 shRNA were transfected with an empty vector or the RNaseH1 expression plasmid. (***, P<0.001 **, P<0.01 *, P<0.05). (F) Phosphorylation of Chk1 and H2A.X were detected via western blot in ADAR1 knockdown cells. ADAR1 knockdown cells were transfected with an empty vector or the RNaseH1 expression plasmid.

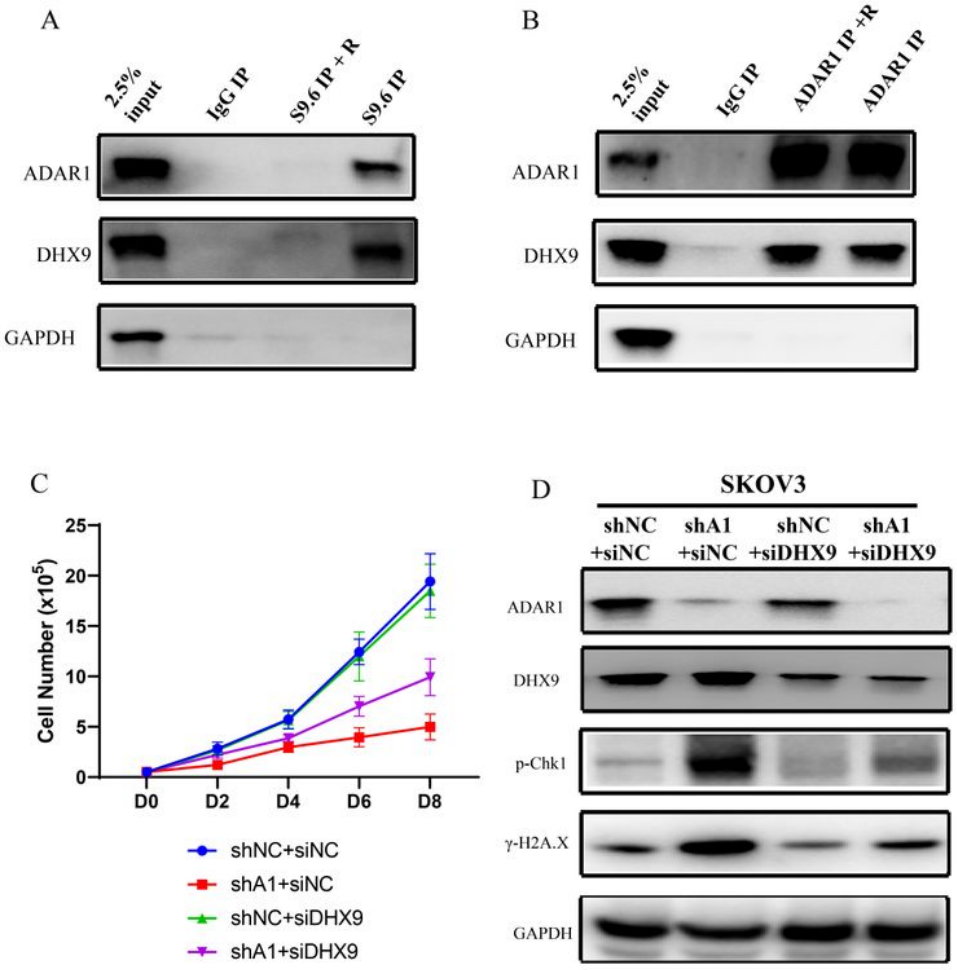

Figure 7

ADAR1 coupled with DHX9 regulate R-Loop accumulation. (A) The interaction between ADAR1 and DHX9 was detected by Co-Immunoprecipitation. (B)The interaction between protein and RNA/DNA was detected by DRIP. (C) Cell growth curve of SKOV3 with scramble shRNA and SKOV3 with ADAR1shRNA. SKOV3 with ADAR1 shRNA were transfected with DHX9 siRNA or not. (D) Phosphorylation of Chk1 and H2A.X were detected via western blot in in ADAR1 knockdown cells. ADAR1 knockdown cells were transfected with DHX9 siRNA or not.

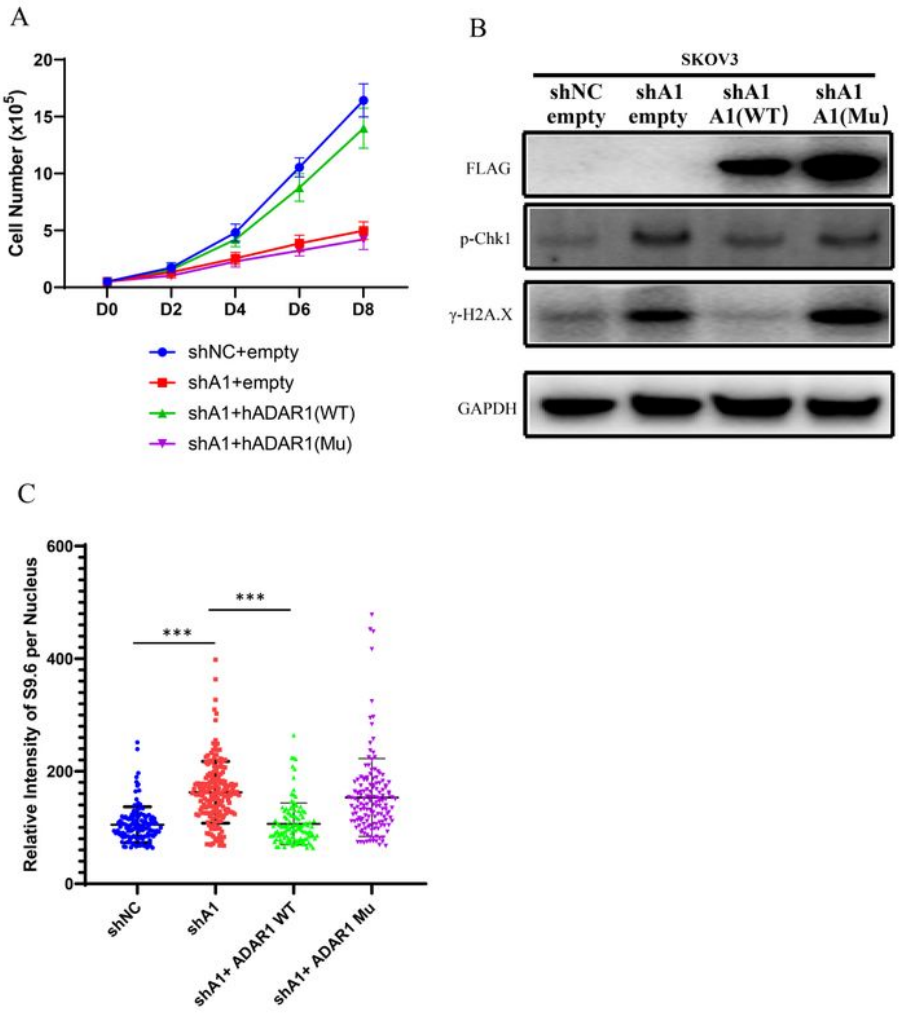

Figure 8

RNA editing regulate R-Loop formation. (A) Cell growth curve of SKOV3 with scramble shRNA and SKOV3 with ADAR1shRNA. SKOV3 with ADAR1 shRNA were transfected with human ADAR1 plasmid or human mutation ADAR1. (B) Phosphorylation of Chk1 and H2A.X were detected via western blot in ADAR1 knockdown cells. ADAR1 knockdown cells were transfected. (C) Quantification of mean intensity of DNA/RNA hybrid (S9.6 antibody) in SKOV3. All data were shown as mean ± SD in n > 90 cells. (***, P<0.001 **, P<0.01 *, P<0.05).

Supplementary Files

This is a list of supplementary files associated with this preprint. Click to download.

- TableS1.xls
- Fig.S1.jpg